Applied Radiation and Isotopes 68 (2010) 755–759

Contents lists available at ScienceDirect

Applied Radiation and Isotopes

journal homepage: www.elsevier.com/locate/apradiso

Evaluation of subject contrast and normalized average glandular dose by semi-analytical models

A. Tomal [a], M.E. Poletti [a,*], L.V.E. Caldas [b]

[a] Departamento de Física e Matemática, Faculdade de Filosofia, Ciências e Letras de Ribeirão Preto, Universidade de São Paulo, Ribeirão Preto, SP, Brazil
[b] Instituto de Pesquisas Energéticas e Nucleares, Comissão Nacional de Energia Nuclear, São Paulo, SP, Brazil

ARTICLE INFO

Keywords:
Mammography
Subject contrast
Detection limits
Normalized average glandular dose

ABSTRACT

In this work, two semi-analytical models are described to evaluate the subject contrast of nodules and the normalized average glandular dose in mammography. Both models were used to study the influence of some parameters, such as breast characteristics (thickness and composition) and incident spectra (kVp and target–filter combination) on the subject contrast of a nodule and on the normalized average glandular dose. From the subject contrast results, detection limits of nodules were also determined. Our results are in good agreement with those reported by other authors, who had used Monte Carlo simulation, showing the robustness of our semi-analytical method.

1. Introduction

Mammography is, nowadays, the most effective and accurate method for early detection of breast cancer. Since mammography is always associated with a small risk of carcinogenesis, it is important to establish an optimization criterion between image quality and breast dose (Dance, 1990; Wu et al., 1991; Dance et al., 2000a). The first step to achieve this optimization is to evaluate the image quality and the absorbed dose in mammography for different examination parameters.

The image quality is usually evaluated in terms of contrast, noise and unsharpness (Carlsson et al., 1986; Vyborny and Schimidt, 1994). In screen–film mammography the image contrast is the main quality index, and it is dependent on subject contrast and on film contrast, which are independent of each other (Wagner, 1991). Several works have investigated the factors that affect the subject contrast (*SC*) of microcalcifications within a breast (Wagner, 1991; Dance et al., 1992, 2000b; Gingold et al., 1995; Delis et al., 2006). However, less extensive data are available for subject contrast of nodules (Wagner, 1991; Yaffe et al., 1994). The subject contrast determination has been performed in most of the previous works by Monte Carlo simulation (Dance et al., 1992; Dance et al., 2000b; Delis et al., 2006), although Carlsson et al. (1986) proposed an analytical model, which could be applied to compute *SC* values in a mammographic examination. A similar semi-analytical model was employed by Leclair and Johns (2002) to compute the contrast only due to scattered radiation.

The average absorbed dose by glandular tissue is the most appropriate information for risk assessments associated with mammography (Dance, 1990; Dance et al., 2000a). However, direct measurement of this quantity is impossible, and in most practical situation it is derived from the product of the measured entrance air kerma and appropriate conversion factors of normalized average glandular dose (Dance, 1990; Wu et al., 1991, 1994; Dance et al., 2000a). These conversion factors can be computed using basically two approaches: from measured depth dose data (Hammerstein et al., 1979) or using Monte Carlo simulation (Dance, 1990; Wu et al., 1991, 1994; Dance et al., 2000a; Koutalonis et al., 2006). Among these methods, the determination by Monte Carlo simulation is the most used, since it eliminates some limitations in the measurements (e.g., variation of the dose laterally, breast phantom composition and geometry).

In summary, these quantities (subject contrast and normalized average glandular dose) are usually determined experimentally and by simulation (Monte Carlo) methods, which are time demanding. Thus the development of analytical models to study these parameters in a fast and simple way would be useful.

In this work, we describe semi-analytic models, which were developed to determine the subject contrast and the normalized average glandular dose in mammography. The model for the subject contrast computation takes into account both primary and scatter (single and double) contributions in the transmitted X-ray intensity. The model for the normalized average glandular dose includes the contribution of single and double interactions in the computation of the fraction of energy absorbed by the glandular tissue. Both semi-analytical models were used to study the influence of some parameters, such as breast characteristics (thickness and composition) and incident spectra (kVp and

* Corresponding author.
E-mail address: poletti@ffclrp.usp.br (M.E. Poletti).

0969-8043/$ - see front matter © 2009 Elsevier Ltd. All rights reserved.
doi:10.1016/j.apradiso.2009.09.040

target–filter combination), on the subject contrast of a nodule and on the normalized average glandular dose. From the subject contrast results, detection limits of nodules were also determined.

2. Materials and methods

2.1. Geometrical model

The compressed breast was represented by a half cylinder, with area of 100 cm^2 and variable thicknesses between 2 and 8 cm. The tissue distribution inside the object was considered as a homogeneous mixture of adipose and glandular tissue uniformly distributed in the central region and enclosed by a 0.5 cm adipose layer in both upper and lower surface. The glandular content of the breast tissue was varied from 0% to 100% in order to represent several breast compositions. The detection system was composed by a Gd_2O_2S:Tb phosphor screen of mass thickness 33.4 mg/cm^2 (compatible with Kodak Min-R 2000) and a Kodak Min-R 2000 film. A 65 cm source-to-image receptor distance was assumed. In this preliminary work the grid was not considered.

For simplicity, two approximations in the geometrical model were adopted. The first one was to assume a parallel beam geometry (i.e., the incident beam was perpendicular and uniformly distributed over the phantom). According to the literature (Boone and Cooper, 2000), this is a good approximation due to small maximum beam divergence in standard mammography. Besides, specifically to study the subject contrast, the large-area contrast approximation was considered, and a contrasting detail with large-area and small thickness (varying between 0.1 and 1 cm) was included within the breast. The contrasting detail (nodule) was composed by malignant breast tissue and was located at an arbitrary distance from the surface.

2.2. Sources of the models: X-ray spectra, compositions data and cross-section

The mammographic spectra utilized in this study were computed using the interpolation polynomial developed by Boone et al. (1997). The X-ray spectra were calculated for Mo and Rh anode materials, operating at tube voltages from 24 to 35 kVp, and filtered with appropriated K-edge filters (Mo and Rh). The spectra were also modified by the addition of a sheet of 3 mm polycarbonate plastic (compression paddle) and normalized to produce the same air kerma of 8.764 mGy. The half value layer (HVL) in mm Al and the mean energy were determined for each spectrum using the model proposed by Kharrati and Zarrad (2003).

The elemental compositions and density of the breast tissues were taken from Hammerstein et al. (1979). The linear attenuation coefficients of the phosphor screen were obtained from the X-COM Database (Berger et al., 2005). Differential cross-sections for the incoherent and coherent scattering were computed using the independent atomic model. The corresponding atomic form factor (F) and incoherent atomic function (S) were obtained from Hubbell et al. (1975).

The linear attenuation coefficients of normal and malignant breast tissues were computed from the parametric curves of Tomal et al. (2009): $\ln(\mu(E)) = a_1 + a_2(\ln E) + a_3(\ln E)^2 + a_4(\ln E)^3$, ($E$ is the energy in keV and $\mu(E)$ is given in cm^{-1}), where the parameters $\{a_1, a_2, a_3$ and $a_4\}$ were determined through least-square technique. The parameters derived from the fitting procedure for each type of breast were for adipose tissue {1.708, 5.060, −3.494, 0.5130}, glandular tissue {−2.410, 10.356, −5.458, 0.7478} and malignant tissue {−2.545, 10.746, −5.620, 0.7665}.

2.3. Subject contrast

The subject contrast (SC) was calculated using Eq. (1), introduced by Carlsson et al. (1986) and Wagner (1991)

$$SC = \ln\left(\frac{q_B}{q_D}\right) \tag{1}$$

where q_B and q_D are the energies imparted to the receptor per unit area beside and behind the contrasting detail, respectively. Considering that these quantities can be separated in primary (p) and scatter (s) components, and assuming that $q_{Bs} = q_{Ds} = q_s$, Eq. (1) becomes

$$SC = \ln\left(1 + \frac{(q_{B_P} - q_{D_P})}{q_{B_P}(q_{D_P}/q_{B_P} + q_s/q_{B_P})}\right) \tag{2}$$

In this work the primary contributions q_{B_P} and q_{D_P} were calculated using Eqs. (3) and (4), previously proposed by Carlsson et al. (1986)

$$q_{B_P} = \int_E E \times \phi_E(E) \times IF(E) \times e^{-\mu_B \cdot L}\, dE \tag{3}$$

$$q_{D_P} = \int_E E \times \phi_E(E) \times IF(E) \times e^{-\mu_B \cdot L} e^{-(\mu_D - \mu_B)x}\, dE \tag{4}$$

where E is the photon energy, $\phi_E(E)$ is the photon fluence, $IF(E)$ is the X-ray detection efficiency, μ_B and μ_D are, respectively, the linear attenuation coefficient of the breast and the contrasting detail, L and x are the thicknesses of the breast and the detail, respectively. The X-ray detection efficiency was estimated as the maximum value, assuming that all photons that interact with the system deposit its energy in a single interaction (i.e., no secondary photons escape), as suggested by Motz and Danos (1978).

The scatter component (q_s) was computed taking into account only the contributions of single and double scattered photon by the breast on the detection system. The single scatter contribution was calculated according to the simple approach proposed by Magalhães et al. (1995), while the double scatter contribution was estimated using the method proposed by Wong et al. (1981). This latter contribution can represent from 15% to 40% of the scatter component (q_s), depending on the breast thickness and composition. The comparison of our $q_S/q_{B_P} (= S/P)$ values with those obtained from Dance et al. (1992) showed a small difference (~7%), demonstrating that the first and second order scatter contributions are the major contributions on the scatter radiation transmitted.

2.4. Normalized average glandular dose

The normalized average glandular dose (D_{gN}) was calculated by,

$$D_{gN} = c \times \frac{1}{w_g \times \rho \times (L - 2a)} \times \left\{ \int E \times \phi_E(E) \times G(E) \times \alpha(E) dE \right\} \tag{5}$$

where c is a unit conversion factor, a is the thickness of the skin layer, ρ and L are the breast density and thicknesses, respectively, $(L - 2a) \times \rho \times w_g$ represents the ratio between the mass of glandular tissue within the breast and the irradiated area, the factor $G(E)$ is used to convert the absorbed energy in the whole breast to the energy absorbed only in the glandular tissue and $\alpha(E)$ is the fraction of incident energy absorbed by the breast. The last two factors were calculated for monoenergetic X-ray beams from 5 to 35 keV in 0.5 keV increments.

The $G(E)$ factors were calculated using the mass energy absorption coefficients (μ_{en}/ρ) for adipose and glandular tissues, as proposed by Boone (1999).

The $\alpha(E)$ fraction was computed considering only the contribution of first and second interactions on the absorbed energy.

Initially, the incident beam (monoenergetic and parallel) was attenuated by the top adipose layer. The energy absorbed in this layer was not included in the dose computation. Then, the central region of the breast was divided into parallel slices, perpendicular to the cylinder symmetry axis. The number of first interactions in each slice was calculated by $N_k(E) = N_0(e^{-\mu \cdot dz(k-1)}) \times (1 - e^{-\mu \cdot dz}) \times (e^{-\mu_s \cdot a})$, where E is the photon energy, μ and μ_s are the linear attenuation coefficients of the breast and adipose layer, respectively, N_0 is the number of incident photons with energy E, dz is the slice thickness and the index k represents the kth slice. The average energy absorbed in the breast due to the first interactions was computed using the relation $E_{1,abs} = \sum_k E \times N_k(E) \times \mu_{en}/\mu$, where μ_{en} is the linear energy-absorption coefficient of the breast. The next step was to compute the energy deposited in the breast due to the second interactions. For this, the number of photons scattered at different directions was determined according to their differential scattering cross sections, and the point of the primary interaction was assumed uniformly distributed on the area perpendicular to the incident beam. The number of second interactions was calculated and the respective absorbed energy $E_{2,abs}$ was numerically evaluated by a similar way to that used to first interactions. Finally, the fraction of absorbed energy due to the first and second interaction, $\alpha(E)$, was computed by $\alpha(E) = (E_{1,abs} + E_{2,abs})/R$, where $R(= N_0 \times E)$ is the radiant energy incident on the breast. It is worth to mention that the contribution of the second interactions on the fraction $\alpha(E)$ represented between 4% and 40% of its value, depending on the breast thickness and photon energy. This large contribution shows the importance of including the second interactions on the D_{gN} values.

3. Results and discussions

3.1. Subject contrast

The influence of the breast thickness and composition on the subject contrast is shown in Fig. 1a, for a nodule of 2 mm and a Mo/Mo target–filter combination at 28 kVp. The subject contrast decreases up to 90% with increasing the breast thickness and glandular content. This can be explained by two facts: the primary contrast decreases due to beam hardening by thicker breasts and the ratio S/P increases for larger thicknesses (Dance et al., 1992, 2000b; Gingold et al., 1995).

Fig. 1b shows the dependency of the subject contrast with the incident spectra for an average breast (50% glandular) of thickness 5 cm and a nodule of 2 mm. The subject contrast is greater for Mo/Mo spectra than for Rh/Rh spectra at lower tube potentials. However, increasing the tube potential from 28 to 35 kVp, the subject contrast decreases up to 35%, 21% and 17% for Mo/Mo, Mo/Rh and Rh/Rh spectrum, respectively. This is attributed to the reduction of the contrast with increasing the mean energy of the spectrum (Gingold et al., 1995). The intersection between the curves, shown in Fig. 1b, is due to the shape of the spectrum transmitted by the breast, and the intersection point depends on the breast thickness and composition.

Finally, based on the results for subject contrast, detection limits were estimated for nodules composed by malignant breast tissue. For this, we considered the screen–film combination described above, and assumed a gross optical density of 1.4 associated with the background, which is a typical value for screen–film mammography. Fig. 2 shows the subject contrast as a function of the nodule size embedded in an average breast of thickness 2, 4, 6 and 8 cm, using a Mo/Mo spectrum at 28 kVp. The threshold values of subject contrast corresponding to differences in optical density between 2% and 6% (these values were determined considering that the human vision can discriminate these differences in optical density) also were included in Fig. 2 in order to illustrate the detection limits. This figure shows detection limits between 1.2 and 3.2 mm for an average breast of 4 cm, depending on the contrast threshold. As breast thickness increases, for 6 and 8 cm, it was observed larger values of detection limit (up to 32 and 68%, respectively). Moreover, the detection limits decrease by a factor of about 2 if the contrasting object is embedded in a pure adipose breast, and increases by a factor about 3 for a pure glandular breast. These results are in agreement to those from Brodie and Gutcheck (1982) (between 2 and 4 mm) and from Del Guerra et al. (2002), determined using a signal-to-noise ratio (SNR) threshold value (between 3 and 5 mm). It is worth to mention that the detection limits presented in this work are valid for large area nodules, with constant thickness (e.g., cubic or cylindrical). For nodules with other geometric shapes (e.g., spherical), the minimum detectable

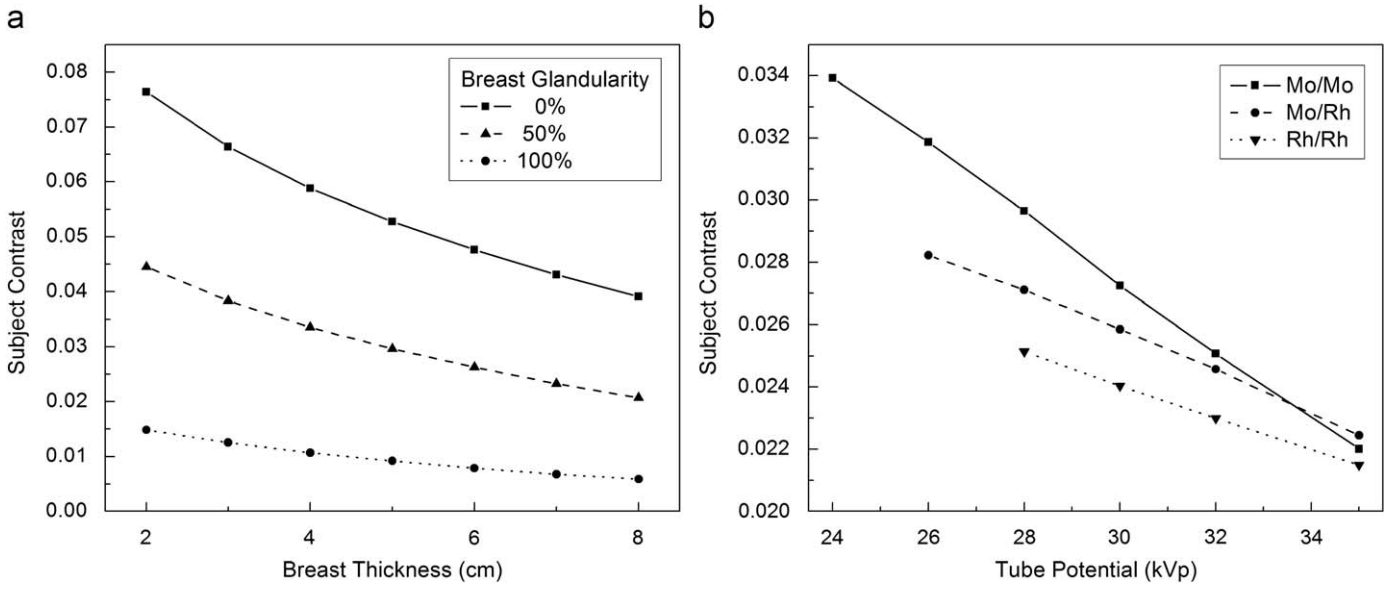

Fig. 1. (a) Subject contrast as a function of the breast thickness and composition, for a nodule of 2 mm and a Mo/Mo spectrum at 28 kVp. (b) Subject contrast as a function of kVp for a breast 50%, adipose 50%, glandular of 5 cm of thickness with a nodule of 2 mm in three different spectra (Mo/Mo, Mo/Rh and Rh/Rh).

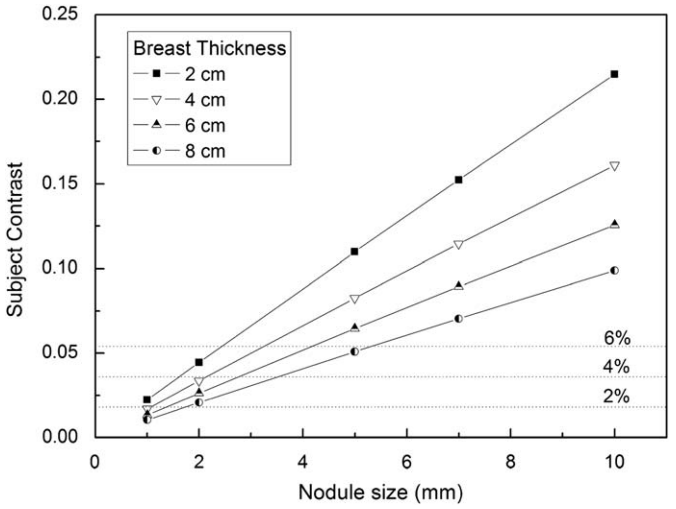

Fig. 2. Subject contrast versus nodule size at average breasts of 2, 4, 6 and 8 cm. (–) represents the contrast thresholds between 2% and 6%.

Table 1
Normalized average glandular dose as a function of breast thickness and compositions.

Breast thickness (cm)	Breast glandularity (%)		
	0	50	100
2.0	0.454	0.411	0.369
3.0	0.345	0.294	0.250
4.0	0.272	0.223	0.183
5.0	0.222	0.176	0.142
6.0	0.185	0.145	0.115
7.0	0.157	0.122	0.097
8.0	0.137	0.105	0.083

Mo/Mo spectrum at 28 kVp (HVL=0.35 mm Al).

detail size can be estimated considering that the detections limits determined previously are related to the mean chord length in these object.

3.2. Normalized average glandular dose

The results for the factors of the normalized average glandular dose as a function of the thickness and composition of the breast are presented in Table 1. The values were calculated for a Mo/Mo spectrum at 28 kVp (HVL=0.35 mm Al). The D_{gN} values decrease with increasing the breast thickness and glandularity by up to 75%. The values of Table 1 were compared with those published by Zoetelief and Jansen (1995), Dance et al. (2000a) and Koutalonis et al. (2006), showing differences $<9\%$. The differences were greater for adipose breast and lesser for glandular breast. These discrepancies can be due to X-ray spectra, geometry, interactions cross-sections, and mainly, due to the semi-analytical approach used to obtain $\alpha(E)$ values. Particularly, it was observed that the differences are higher for thicker breasts. This was expected because our model neglects the multiple scattering that becomes more probable with increasing the breast thickness.

The influence of the incident spectra on D_{gN}-factors is presented in Table 2 for an average breast (50% glandular) of 5 cm. For a given kVp and anode–filter combination, the D_{gN} values increase up to 9% with increasing the HVL, as presented in Table 2. For the complete range studied in this work, a large variation (up to 20%) with the HVL was found. The D_{gN} values also increase with the kVp. Although the variation presented in Table 2 is small, the differences can be up to 10% for a large alteration in kVp and constant HVL. From Table 2, it can be seen that the D_{gN} values for a Mo/Mo spectra are smaller than for Mo/Rh and Rh/Rh by approximately 3% and 8%, respectively. In summary, the general behaviors of our data are in agreement with observation of Wu et al. (1991, 1994) and Dance et al. (2000a).

Table 2
Influence of the incident spectra on the normalized average breast dose for an average breast (50% glandular) of 5 cm.

(kVp)	HVL (mm Al)	Anode–filter combination		
		Mo/Mo	Mo/Rh	Rh/Rh
26	0.36	0.182	0.188	–
28	0.36	0.186	0.192	0.200
	0.38	0.194	0.200	0.208
	0.40	0.202	0.209	0.218
30	0.40	0.204	0.210	0.221
32	0.42	0.214	0.220	0.234

4. Conclusions

In this work we illustrated two semi-analytic models that provide a simple and accurate way to calculate subject contrast and normalized average glandular dose in mammography. Both semi-analytical models were used to study the influence of some parameters, such as breast characteristics (thickness and composition) and incident spectra (kVp and target–filter combination) on the subject contrast of a nodule and on the normalized average glandular dose. The obtained results are in good agreement with those reported by others authors, who had used Monte Carlo simulation (Dance, 1990; Wu et al., 1991, 1994; Zoetelief and Jansen, 1995; Dance et al., 2000a). These facts show that higher orders of interactions can be neglected without inducing large errors compared with Monte Carlo simulations, and simplifying the analytical models. However, for large breasts, the developed models could be improved, including interactions of higher orders, in order to provide more precise results of subject contrast and normalized average glandular dose. Finally, this study allows predictions of detection limits for nodules embedded in breast of different thickness and composition.

Regarding to the limitations of the semi-analytical models described in this work, we can cite the use of a parallel beam geometry (which can underestimate the *SC* and D_{gN} values up to 1%), the use of a non-finite focal spot (which excludes another effects on the image quality, such as unsharpness), and the definition of detection limits from the large area contrast. Therefore, in order to reduce the simplifications adopted further studies must be performed, attempting to improve the irradiation geometry (considering a finite focal spot and a divergent beam), and to extend the definition of detection limits (combining threshold values of contrast and signal-to-noise ratio).

Acknowledgments

This work was supported by the Brazilian agencies Coordenação de Aperfeiçoamento de Pessoal de Nível Superior (CAPES), Fundação de Amparo à Pesquisa do Estado de São Paulo (FAPESP), and Conselho Nacional de Desenvolvimento Científico e Tecnológico (CNPq).

References

Berger M.J., Hubbell J.H., Seltzer, S.M., Chang, J., Coursey, J.S., Sukumar, R., Zucker, D.S., 2005. XCOM: photon cross section database (version 1.3). Available at 〈http://physics.nist.gov/xcom〉.

Boone, J.M., Fewell, T.R., Jennings, R.J., 1997. Molybdenum, rhodium, and tungsten anode spectral models using interpolation polynomials with application to mammography. Med. Phys. 24, 1863–1875.

Boone, J.M., Cooper, V.N., 2000. Scatter/primary in mammography: Monte Carlo validation. Med. Phys. 27, 1818–1831.

Boone, J.M., 1999. Glandular breast dose for monoenergetic and high-energy X-ray beams: Monte Carlo assessment. Radiology 213, 23–37.

Brodie, I., Gutcheck, R.A., 1982. Radiographic information theory and application to mammography. Med. Phys. 9, 79–94.

Carlsson, G.A., Carlsson, C.A., Nielsen, B., Persliden, J., 1986. Generalized use of contrast degradation and contrast improvement factors in diagnostic radiology, application to vanishing contrast. Phys. Med. Biol. 31, 737–749.

Dance, D.R., 1990. Monte Carlo calculation of conversion factors for the estimation of mean glandular breast dose. Phys. Med. Biol. 35, 1211–1219.

Dance, D.R., Persliden, J., Carlsson, G.A., 1992. Calculation of the dose and contrast for two mammographic grids. Phys. Med. Biol. 37, 235–248.

Dance, D.R., Skinner, C.L., Young, K.C., Beckett, J.R., Kotre, C.J., 2000a. Additional factors for the estimation of mean glandular breast dose using the UK mammography dosimetry protocol. Phys. Med. Biol. 45, 3225–3240.

Dance, D.R., Klang, A.T., Sandborg, M., Smith, A.C., Carlsson, G.A., 2000b. Influence of anode/filter material and tube potential on contrast, signal-to-noise ratio and average absorbed dose in mammography: a Monte Carlo study. Br. J. Radiol. 73, 1056–1067.

Del Guerra, A., Belcari, N., Bencivelli, W., Motta, A., Righi, S., Vaiano, A., Di Domenico, G., Moretti, E., Sabba, N., Zavattini, G., Campanini, R., Lanconelli, N., Riccardi, A., Cinti, M.N., Pani, R., Pellegrini, R., 2002. Monte Carlo study and experimental measurements of breast tumor detectability with the YAP-PEM prototype. IEEE Trans. Nucl. Sci. 3, 1887–1891.

Delis, H., Spyrou, G., Costaridou, L., Tzanakos, G., Panayiotakis, G., 2006. Suitability of new anode materials in mammography: dose and subject contrast considerations using Monte Carlo simulation. Med. Phys. 33, 4221–4235.

Gingold, E.L., Wu, X., Barnes, G.T., 1995. Contrast and dose with Mo–Mo, Mo–Rh and Rh–Rh target–filter combinations in mammography. Radiology 195, 639–644.

Hammerstein, G.R., Miller, D.W., White, D.R., Masterson, M.E., Woodard, H.Q., Laughlin, J.S., 1979. Absorbed radiation dose in mammography. Radiology 130, 485–491.

Hubbell, J.H., Veigele, W.J., Briggs, E.A., Brown, R.T., Cromer, D.T., Howerton, R.J., 1975. Atomic form factors, incoherent scattering functions and photon scattering cross sections. J. Phys. Chem. Ref. Data 4, 471–538.

Kharrati, H., Zarrad, B., 2003. Computation of beam quality parameters for Mo/Mo, Mo/Rh, and W/Al target/filter combinations in mammography. Med. Phys. 30, 2638–2642.

Koutalonis, M., Delis, H., Spyrou, G., Costaridou, L., Tzanakos, G., Panayiotakis, G.., 2006. Monte Carlo generated conversion factors for the estimation of average glandular dose in contact and magnification mammography. Phys. Med. Biol. 51 (21), 5539–5548.

Leclair, R.J., Johns, P.C., 2002. Optimum momentum transfer arguments for X-ray forward scatter imaging. Med. Phys. 29, 2881–2890.

Magalhães, S.D., Eichler, J., Gonçalves, O., 1995. Calculation on X-ray scattering of 17.4 keV radiation and image degradation in mammography. Nucl. Instrum. Methods B 95, 87–90.

Motz, J.W., Danos, M., 1978. Image information content and patient exposure. Med. Phys. 5, 8–22.

Tomal, A., Mazarro, I., Kakuno, E.M., Poletti, M.E., 2009. Experimental determination of linear attenuation coefficient of normal, benign and malignant breast tissues. Radiat. Phys. Chem., submitted for publication.

Vyborny, C.J., Schimidt, R.A., 1994. Technical image quality and the visibility of mammographic detail. RSNA Categorical Course in Phys., 103–111.

Wagner, A.J., 1991. Contrast and grid performance in mammography. In: Barnes, G.T., Frey, G.D. (Eds.), Screen Film Mammography: Imaging Considerations and Medical Physics Responsibilities, Madison, WI, Med. Phys. 25, pp. 115–134.

Wong, J.W., Henkelman, R.M., Fenster, A., Johns, H.E., 1981. Second scatter contribution to dose in a Co-60 beam. Med. Phys. 8, 775–782.

Wu, X., Barnes, G.T., Turker, D.M., 1991. Spectral dependence of glandular tissue dose in screen–film mammography. Radiology 179, 143–148.

Wu, X., Barnes, G.T., Gingold, E.L., Turker, D.M., 1994. Normalized average glandular dose in molybdenum target–rhodium filter and rhodium target–rhodium filter mammography. Radiology 193, 83–89.

Yaffe, M.J., Jennings, R.J., Fahrig, R., Fewell, T.R., 1994. X-ray spectral considerations for mammography. RSNA Categorical Course Phys., 63–73.

Zoetelief, J., Jansen, J.T.M., 1995. Calculation of air kerma to average glandular tissue dose conversion factors for mammography. Radiat. Prot. Dosim. 57, 397–400.